nature communications

Article

https://doi.org/10.1038/s41467-025-59027-3

Heterocycle-based dynamic covalent chemistry for dynamic functional materials

Received: 30 October 2024

Accepted: 7 April 2025

Published online: 17 April 2025

Check for updates

Zeyu Ma[1], Siyu Pan[1], Yang Yang[2], Yuan Zeng[1], Bo Wang[3] ✉, Yen Wei[1] & Lei Tao[1] ✉

Dynamic covalent chemistry, which renders reusable and degradable thermoset polymers, is a promising tool for solving the global problem of plastic pollution. Although dynamic covalent chemistry can construct dynamic polymer networks, it rarely introduces other functions into polymers, which limits the development of dynamic functional materials. Herein, we develop heterocycle-based dynamic covalent chemistry and demonstrate the reversibility of the aza-Michael addition reaction between functional heterocycle dihydropyrimidin-2(1*H*)-thione and electron-deficient olefins. Our method produces a degradable linear polymer and recyclable and self-healable cross-linked polymers similar to traditional dynamic covalent chemistry, but the heterocycles endow the polymer with excellent ultraviolet-blocking and high-energy blue light-blocking abilities, and tunable fluorescence and phosphorescence properties. These are difficult to create with ordinary dynamic covalent chemistry. This proof-of-concept study provides insights into heterocycle-based dynamic reactions, and may prompt the development of dynamic chemistry and dynamic functional materials.

Thermoset polymers, synthesized through dynamic covalent chemistry (DCC), have novel properties such as reusability, recyclability, degradability, and self-healing capabilities[1–4], that meet the "three Rs" (reduce, reuse, and recycle) of sustainable development. Thus, using DCC to fabricate dynamic polymers is considered to be a promising solution to the plastic pollution problem, which is of global concern[5–7]. In recent decades, many elegant and dynamic polymer materials have been developed through a series of dynamic reactions, including transesterification[8–12], transalkylation[13–15], transamination[16–20], and the Michael addition reaction[21–25]. However, current dynamic reactions endow polymer materials with adaptive networks but have only a few functions. They must be combined with other reactions for dynamic functional materials to be developed, thus increasing the difficulty and complexity of material design and preparation. Therefore, the exploration of dynamic reactions based on structures that possess unique functions is important to the development of DCC and dynamic functional materials, and finding functional groups that are capable of supporting dynamic reactions is key to this exploration.

Heterocyclic compounds have many important functions and play essential roles in material science, biological science, and the medical field[26–28]. However, dynamic reactions based on the functional heterocycle are rarely exploited for the development of dynamic polymer materials. Here, we explore heterocycle-based DCC (H-DCC) by demonstrating a dynamic reaction based on the 3,4-dihydropyrimidin-2(1*H*)-thione (DHPMT) heterocycle (Fig. 1a) and developing related dynamic functional materials (Fig. 1b).

We present DHPMT as a typical example of heterocycles for the following reasons: (i) Some aza-Michael addition reactions are reversible[21,29]; thus, the efficient aza-Michael addition reactions between DHPMT and electron-deficient olefins[30,31] may be reversible under carefully screened conditions, although their reversibility has not yet been reported. (ii) DHPMT derivatives have many useful properties, such as anti-ultraviolet (UV), anti-bacterial, anti-viral, and

[1]The Key Laboratory of Bioorganic Phosphorus Chemistry & Chemical Biology (Ministry of Education), Department of Chemistry, Tsinghua University, Beijing 100084, P. R. China. [2]Institute of Nuclear and New Energy Technology, Tsinghua University, Beijing 100084, China. [3]Institute of Food Science and Technology, Chinese Academy of Agricultural Sciences, Beijing 100193, China. ✉e-mail: youxihema@gmail.com; leitao@tsinghua.edu.cn

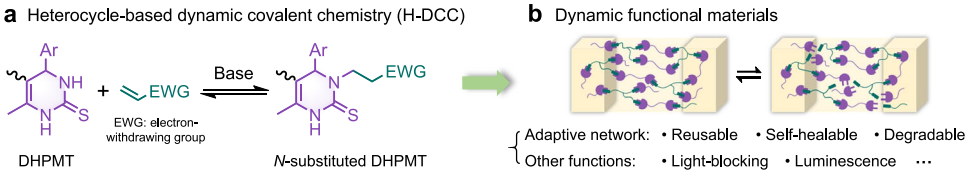

Fig. 1 | Heterocycle-based dynamic covalent chemistry (H-DCC). a Heterocycle-based dynamic covalent chemistry (3,4-dihydropyrimidin-2(1*H*)-thione (DHPMT) as a typical example) developed in this work. **b** DHPMT-based reversible reaction for the facile fabrication of dynamic functional materials.

anti-oxidation[32,33]; thus, they can be used for developing dynamic functional materials if the retro-aza-Michael addition reaction is available under the given conditions. (iii) DHPMT derivatives having different structures and functions can be facilely prepared via the famous three-component Biginelli reaction using accessible substrates; thus, the target dynamic materials can be prepared with tunable functions and at low synthetic costs.

We investigated the thermodynamic and kinetic properties of the aza-Michael addition reactions between DHPMT and different electron-deficient olefins, and we selected acrylate as a typical olefin with which to explore the conditions that were favorable for the reverse reaction and to uncover the mechanism. Within 4 h, the linear polymer prepared by the step-growth polymerization of di-acrylate and di-DHPMT monomers had almost completely depolymerized into monomers under the screened conditions, thus demonstrating that this polymer could serve as a degradable polymer. A bulk material prepared using di-DHPMT and commercial tri-acrylate monomers demonstrated recyclability and dynamic properties, as well as the characteristics of a fast relaxation rate (τ~1min) and activation energy ($E_a = 36.2 \pm 1.5$ kJ mol^{-1}) that was close to the lowest reported value (31 ± 10 kJ mol^{-1}). The polymer film prepared with this dynamic material showed self-healing ability at room temperature (25 °C, recovery rate: ~90% after 10 min). It also offered excellent UV-blocking capacity (blocking rate: > 99% for UV light) while maintaining high transparency (87% for visible light) due to the heterocyclic structure of the polymer network. This transparent and full-band UV-resistant dynamic material is difficult to achieve with traditional DCC. By simply changing the aldehyde component involved in the Biginelli reaction, we facilely altered the structure of the di-DHPMT monomer and, using this monomer, developed another self-healable polymer film that was superior, in terms of high-energy blue light (HEBL)-shielding ability (97% at 450 nm) and transparency (92% at 650 nm), to other recently reported materials. These UV-blocking and HEBL-blocking films also exhibited tunable fluorescence and phosphorescence properties, which indicated their potential as optical materials. These results further demonstrate the advantages of H-DCC in facilely exploring dynamic functional materials.

Results

Previous reports on the aza-Michael addition reaction between DHPMT and electron-deficient olefins have rarely mentioned that such a reaction is reversible[30,31]. Here, we studied the types of olefin substrates and the thermodynamic and kinetic properties of the reaction in detail to explore its reversibility under certain conditions. We used benzyl acrylate (**a**, Fig. 2a) and a DHPMT model compound (M0, Fig. 2a) to optimize the conditions for the addition, including solvent, temperature, base type, and base amount (Supplementary Section 4.1), and we used ^{1}H nuclear magnetic resonance (NMR) to monitor the reactions.

The addition reaction proceeded smoothly in a heated polar aprotic solvent (dimethyl sulfoxide (DMSO) or *N*,*N*-dimethylformamide (DMF)) catalyzed by medium-strong bases (K_2CO_3 or 1,8-diazabicyclo[5.4.0]undec-7-ene (DBU), 10 mol% to DHPMT) (Supplementary Tables 1–4). Then, we reacted different kinds of electron-deficient olefins (**a**–**j**, Fig. 2a) with M0 under the same conditions. Benzyl acrylate (**a**), benzyl methacrylate (**b**), *N*-benzylacrylamide (**c**), phenyl vinyl sulfone (**d**), and acrylonitrile (**e**) smoothly produced the expected 1,4-adducts, but *N*-benzylmethacrylamide (**f**), ethyl crotonate (**g**), *N*-phenylmaleimide (**h**), maleic anhydride (**i**), and 2-cyclohexen-1-one (**j**) did not produce the target product. These results indicate that only olefins with an unsubstituted methylene end group are potentially viable for the addition reaction.

We determined the values of the standard equilibrium constant ($K^{\ominus}_{add}$) and the equilibrium time ($t_{add,\,eq}$) of the addition reaction at 100 °C from the ^{1}H NMR data. The reactions between M0 and **a**–**e** reached equilibrium after different time periods ($t_{add,\,eq}$ = 2–540 min), and the equilibrium conversions were less than 99% ($K^{\ominus}_{add}$ = 2.6–1 × 10^4) (Supplementary Table 5). These results imply that these reactions have potential reversibility under the established conditions.

We designed exchange reactions to investigate the reversibility of the addition reactions between M0 and the five olefin substrates (**a**–**e**) (Fig. 2b, top). The exchange reactions involving the adducts of **a, b, d**, and **e** proceeded smoothly at fast rates (k_{ex} = 0.0072–0.010 L mol^{-1} min^{-1}), as calculated from the ^{1}H NMR data (Fig. 2b, bottom; Supplementary Section 4.3). However, no exchange reaction was observed for M0-**c**. These results demonstrate that the substrates acrylate, methacrylate, vinyl sulfone, and acrylonitrile are suitable for reacting with DHPMT to form decomposable products.

Next, we used M0-**a** to react with various DHPMT derivatives (M1, M2, and M3) to assess the universality of the reversible reaction (Supplementary Fig. 1 and Supplementary Section 4.3). The model compounds M1, M2, and M3 were synthesized by altering different modules of the Biginelli reaction (Supplementary Fig. 2). As a typical example, the ^{1}H NMR data for the exchange reaction between M2 and M0-**a** are presented, and the characteristic methine peaks of M0-**a** (5.55 ppm), M2 (5.20 ppm), M2-**a** (5.73 ppm), and M0 (5.17 ppm) are marked in Fig. 2c. M2-**a** and M0 increased over time, whereas M0-**a** and M2 decreased until equilibrium was reached within 150 min. The results of the kinetic study agreed well with an apparent second-order reversible reaction model (Supplementary Section 4.3); the equilibrium constant and the apparent kinetic constant were estimated (Supplementary Table 6). When M1 and M3 were used, the exchange reactions smoothly proceeded at different rates and reached equilibrium within 240 min (Supplementary Figs. 3, 4). These results demonstrate that altering the structures of DHPMT affects the exchange rates and equilibrium conversions while maintaining the dynamic nature of the reaction. Thus, we may design DHPMT derivatives having different structures to develop function-tunable dynamic polymers.

We also examined the exchange reaction of M0-**a** and M2 at ambient temperatures (Supplementary Fig. 5). At room temperature (25 °C), the conversion of the exchange reaction was 3% after 24 h. At 30 °C, the conversion increased to 10%. Besides the exchange reaction between the Michael adduct and DHPMT derivative, we further investigated the reaction of two Michael adducts (Supplementary Fig. 6). The conversion of this exchange reaction was 5% at 25 °C and 6% at 30 °C after 24 h, respectively. These results demonstrate that the dynamic bonds are reversible at ambient temperatures.

To gain a deep understanding of the reversible exchange reaction, we performed density functional theory (DFT) simulations to elucidate the mechanism (Fig. 2d; Supplementary Section 4.5). Our simulations

https://doi.org/10.1038/s41467-025-59027-3

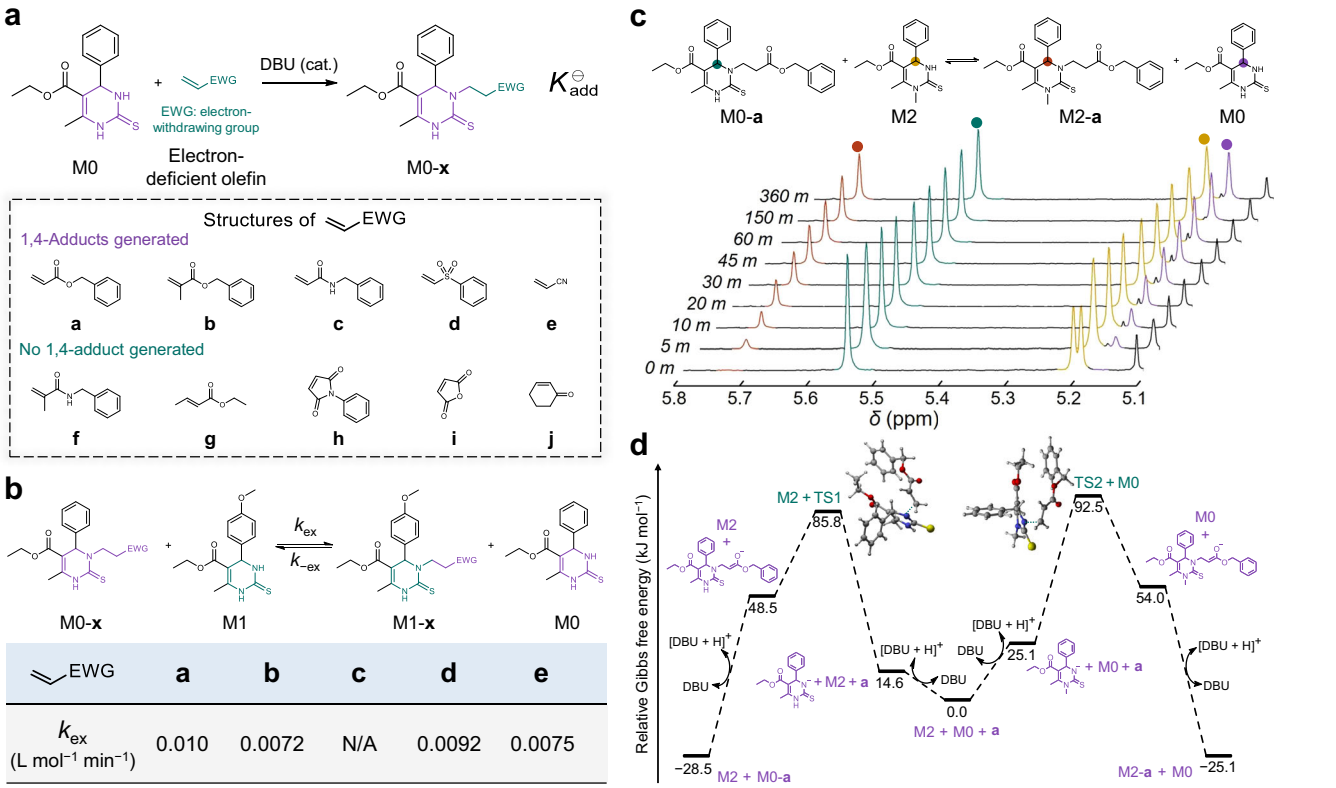

EWG	a	b	c	d	e
k_{ex} (L mol^{-1} min^{-1})	0.010	0.0072	N/A	0.0092	0.0075

Fig. 2 | Model study and mechanism of the DHPMT-based reversible reactions. **a** Model addition reactions between M0 and different electron-deficient olefins (**a**–**j**). Reaction conditions: c(M0) = c(olefin) = 2 M, 10 mol% DBU in DMF, 100 °C. **b** Exchange reaction between M0-**x** (**x** = **a, b, c, d**, **e**) and M1, and corresponding apparent kinetic constants (k_{ex}) for the forward reaction. Reaction conditions: c(M0-**x**) = c(M1) = 1 M, 10 mol% DBU in DMF, 100 °C. **c** Exchange reaction between M0-**a** and DHPMT derivative M2 and corresponding ^{1}H NMR (400 MHz, DMSO-d_6) spectra at different time intervals. Reaction conditions: c(M0-**a**) = c(M2) = 1 M, 10 mol% DBU in DMF, 100 °C. **d** Gibbs free energy profiles of the exchange reaction between M0-**a** and M2 via theoretical rationalization. The spatial configurations of the transition states (TSs) are shown.

reveal that the exchange reaction follows a retro-addition and Michael addition pathway. DBU deprotonates M0-**a** to form an anion to initiate the reaction. The cleavage of the C-N bond leads to the formation of transition state 1 (TS1, ΔG_{TS1} = 85.8 kJ mol^{-1} relative to the intermediate state). Then, the intermediate products M0 and **a** are generated through successive exothermic processes involving C-N bond cleavage and protonation, consistent with the observed formation of acrylate during the exchange reaction (Supplementary Fig. 7). The subsequent Michael addition reaction occurs via a reverse pathway: the alkene group in **a** approaches the M2 anion from above the twist-boat-form heterocycle to form transition state 2 (TS2, ΔG_{TS2} = 92.5 kJ mol^{-1} relative to the intermediate state). After C-N bond formation and protonation, the final products M2-**a** and M0 are generated. The exchange reaction follows a base-catalyzed retro-addition/aza-Michael addition mechanism. This differs from the aza-Michael addition mechanism of common amines, which usually undergoes a cation-involved pathway.

The theoretical Gibbs free energy of activation ($\Delta G^{\ddagger}$ (theo)) for the exchange reaction was calculated to be 121.0 kJ mol^{-1}, which was higher than the experimental value ($\Delta G^{\ddagger}$(exp) = 77.3 kJ mol^{-1}) obtained through kinetic studies (Supplementary Section 4.4). This deviation could be contributed to that the simplified transition state model used in the theoretical calculation cannot fully simulate the complex multi-component process of the exchange reaction.

We also investigated the mechanism of the addition reaction of M0 and **a**. The DBU-catalyzed addition reaction was exothermic; thus, the elevated temperature was conducive to the reverse reaction (Supplementary Fig. 8). The theoretical change in reaction enthalpy (ΔH_a(theo) = −28.5 kJ mol^{-1}) closely matched the experimental value (ΔH_a(exp) = −39.5 kJ mol^{-1}; Supplementary Section 4.6). Additionally, the triethylamine (TEA)-catalyzed addition reaction (Supplementary Fig. 9) had higher energy barriers for both the addition reaction (ΔG_a(TEA) = 118.4 kJ mol^{-1}) and the retro-addition reaction (ΔG_{ra}(TEA) = 146.9 kJ mol^{-1}) than did the DBU-catalyzed reaction (ΔG_a(DBU) = 85.8 kJ mol^{-1}; ΔG_{ra}(DBU) = 114.3 kJ mol^{-1}), which was consistent with the experimental results (Supplementary Table 3) and indicated that a stronger base favors a lower energy barrier. These DFT simulation results provide comprehensive insights into the mechanism of the exchange reaction and reveal the conditions favoring the reverse reaction, thus offering theoretical illustrations for the dynamic behavior in bulk materials and informing the reaction conditions for the following experiments.

Considering the results of the model experiments and the accessibility of the substrate, we selected acrylate as the optimized olefin substrate for polymer preparations. We have used the efficient addition reaction between DHPMT and acrylate for step-growth polymerization in our previous work[34]. Here, we prepared the linear polymer P1 (M_n(gel permeation chromatography, GPC) = 1.9 × 10^4 g mol^{-1}, PDI = 1.9) using di-acrylate (A_2) and di-DHPMT (B_2) monomers as in the previous method, and we then investigated its degradation (Fig. 3a, top). The retro-aza-Michael addition reaction has been favored by dilution, heating, and strong base as a catalyst according to the results of the abovementioned experiments and DFT simulation; thus, we prepared a dilute solution of P1 (1.0 mM in DMF or DMSO-d_6, calculated as monomer units) and heated the solution to 120 °C. The strong base sodium *tert*-butoxide (^{t}BuONa) was added as the catalyst to reduce the energy barrier of the retro-addition reaction. GPC analyses demonstrated the rapid degradation of P1 to oligomers within 5 min, and the large-molecular-weight

https://doi.org/10.1038/s41467-025-59027-3

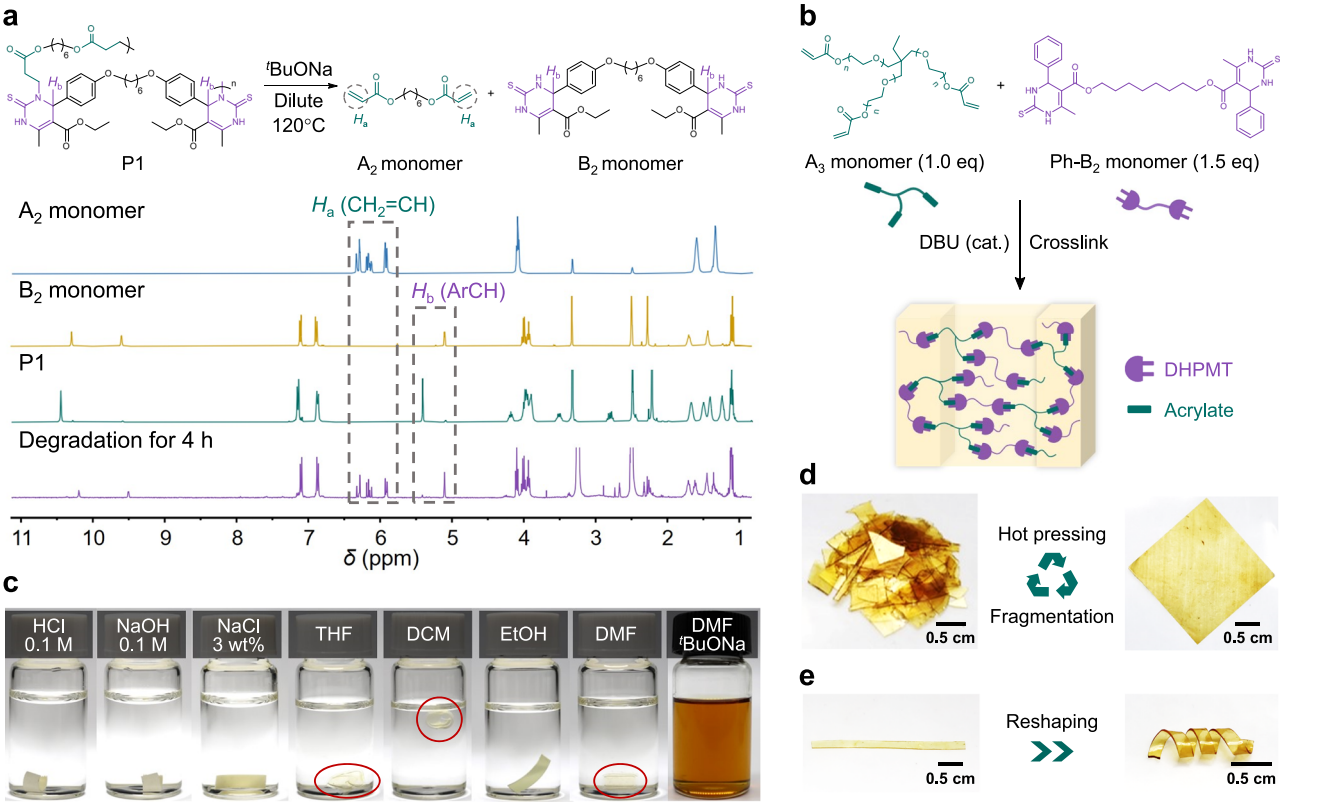

Fig. 3 | Dynamic property of DHPMT-acrylate polymers. a Linear polymer P1 prepared by A_2 and B_2 monomers and its degradation (top) and comparative ^{1}H NMR (400 MHz, DMSO-d_6) analyses of A_2 monomer, B_2 monomer, P1, and the mixture after 4 h of degradation, respectively (bottom). Conditions: 120 °C, 1.0 mM P1 (calculated as monomer units) with 1 eq sodium *tert*-butoxide (^{t}BuONa) in DMSO-d_6 (for NMR analysis) or DMF (for gel permeation chromatography (GPC) analysis). **b**, Preparation of the crosslinked bulk material (Ph polymer) from phenyl-substituted di-DHPMT monomer (Ph-B_2 monomer, 1.5 eq) and commercially available tri-acrylate monomer (A_3 monomer, 1.0 eq, molar mass $M(A_3)$ = 428, 692, or 912 g mol^{-1}) under the catalyzation of DBU (0.225 eq). **c** Ph polymer ($M(A_3)$ = 692 g mol^{-1}) in various solvents. Samples in some solvents are marked by red circles. THF tetrahydrofuran, DCM dichloromethane, EtOH ethanol, DMF *N*,*N*-dimethylformamide. **d** Reprocessing of the Ph polymer ($M(A_3)$ = 428 g mol^{-1}) by hot pressing at 180 °C. Scale bar = 0.5 cm. **e** Reshaping of the Ph polymer ($M(A_3)$ = 692 g mol^{-1}) at 100 °C. Scale bar = 0.5 cm.

peak decreased over time and became undetectable after 4 h (Supplementary Fig. 10).

In the ^{1}H NMR spectra (Fig. 3a, bottom), signals (5.87–6.36 ppm) appeared in the same position as the alkene peaks of the A_2 monomer (H_a) after the degradation. Meanwhile, the methine peak (H_b) of P1 (5.42 ppm) was shifted to 5.10 ppm, which was consistent with the characteristic methine peak of the B_2 monomer. These results indicate that the linear polymer P1 can be almost completely degraded into monomers, and that it is a potential eco-friendly polymer.

We then prepared crosslinked polymers with dynamic DHPMT-acrylate networks (Fig. 3b; Supplementary Section 4.8). A commercial tri-acrylate monomer (A_3 monomer, 1.0 eq) and a phenyl-substituted di-DHPMT monomer (Ph-B_2 monomer, 1.5 eq) were mixed with equivalent reaction groups to ensure a high crosslink density. The mixture was heated to homogeneous on a thermal plate (160 °C), and then DBU (0.225 eq, i.e., 0.075 eq to DHPMT) was added as the catalyst to initiate the polymerization. A polymer network (Ph polymer) rapidly formed (~10 min) at 160 °C. In solid-state cross-polarization magic-angle spinning (CP/MAS) NMR spectra, the vinyl signal of the A_3 monomer almost disappeared, indicating that the crosslinking reaction was nearly complete (Supplementary Fig. 11a). The transverse relaxation decay curve by low-field NMR demonstrated that the crosslinked polymer was almost entirely composed of crosslinked chains with few dangling or free chains, indicating a high crosslinking density (Supplementary Fig. 11b; Supplementary Section 4.9).

The Ph polymer exhibited excellent chemical resistance in 0.1 M HCl (aq), 0.1 M NaOH (aq), 3 wt% NaCl (aq), tetrahydrofuran (THF), dichloromethane (DCM), ethanol (EtOH), and DMF (Fig. 3c; Supplementary Section 4.10). The gel contents determined through the use of each of the solvents were greater than 97% due to the highly crosslinked polymer network (Supplementary Table 8). Notably, the Ph polymer was completely dissolved in hot DMF (80 °C, 8 h) when ^{t}BuONa (0.1 eq to DHPMT) was added (Fig. 3c). ^{1}H NMR and GPC analyses indicated that the crosslinked Ph polymer was depolymerized into a low molecular weight polymer (M_n(GPC) = 8.8 × 10^3 g mol^{-1}, PDI = 2.3) via the retro-Michael addition reaction pathway (Supplementary Fig. 12). Furthermore, the degraded polymer was successfully repolymerized, yielding a recycled crosslinked polymer (yield: ~95%) (Supplementary Section 4.11). Compared with the original polymer, the recycled polymer had a similar glass transition temperature (T_g) (Supplementary Fig. 13a) and thermal stability below 400 °C (Supplementary Fig. 13b); however, its thermal stability above 400 °C and mechanical strength changed (Supplementary Fig. 13c). These results demonstrate that the Ph polymer is recyclable under suitable conditions while side products may be generated during the recycling process.

We then reprocessed and reshaped the Ph polymers to test their dynamic properties (Supplementary Section 4.12). Fragments of the polymer could conveniently be reprocessed repeatedly into a uniform film by hot pressing (Fig. 3d); the shape of the polymer material could be changed at an elevated temperature and then fixed at room temperature (25 °C, Fig. 3e). These results suggest that this polymer material crosslinked via DHPMT-acrylate has dynamic properties similar to those of other dynamic materials.

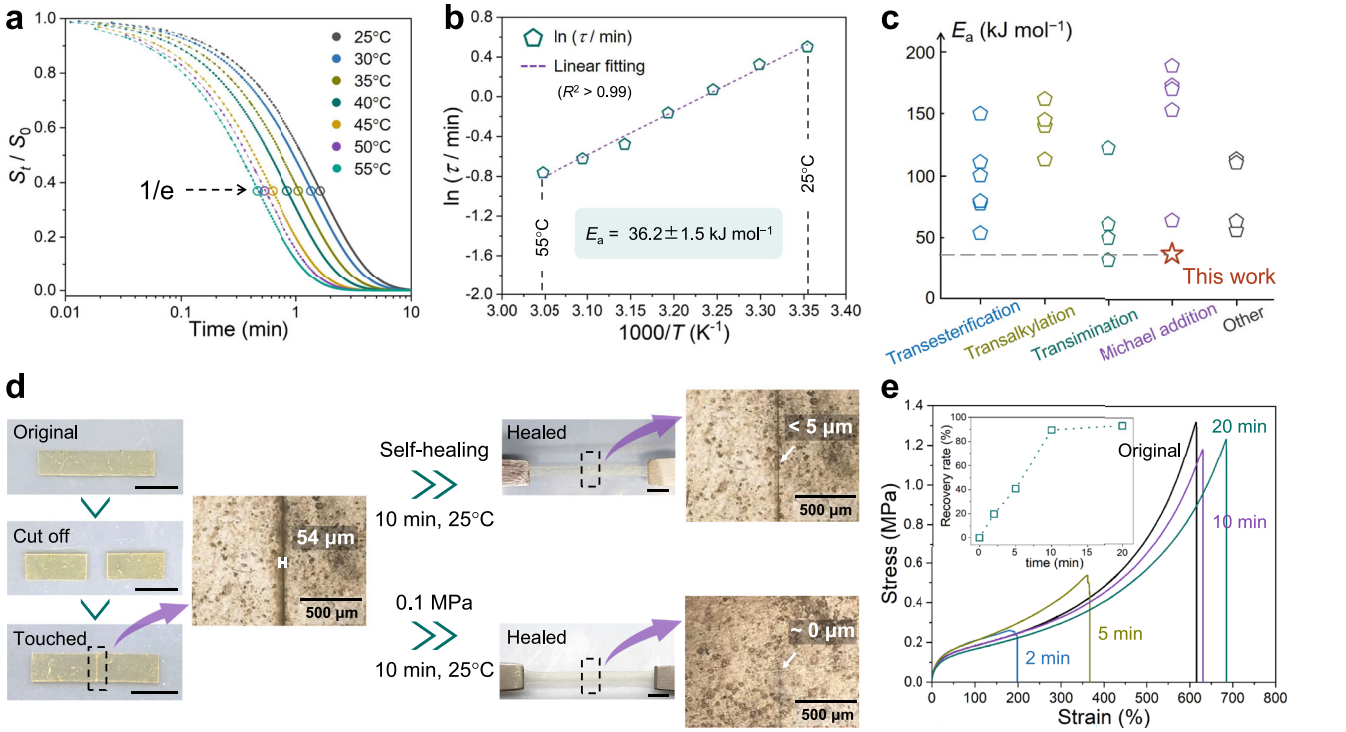

Fig. 4 | Stress relaxation and self-healing tests of the Ph polymer. a Stress relaxation tests for the Ph polymer ($M(A_3)$ = 692 g mol^{-1}) at different temperatures by dynamic mechanical analysis, with the results fitted by an exponential equation. The time when S_t/S_0 reached 1/e was defined as the relaxation time (τ). **b** Arrhenius plot to determine the activation energy (E_a) of stress relaxation (coefficient of determination R^2 = 0.991). **c** Comparison of the Ph polymer with reported DCC-based materials in terms of the E_a of stress relaxation. **d** Photos and microscopic observations of the self-healing (top) and healing under pressure (~0.1 MPa, bottom) of the Ph polymer at room temperature (25 °C); dashed box: the position of the crack; scale bar of photos = 0.5 cm; scale bar of microscopic images = 500 μm. **e** Mechanical stiffness characterization of samples after different durations of self-healing and corresponding mechanical recovery rate calculated from the breaking stress value (inset).

To further study the dynamic properties of this material, we performed stress relaxation tests at various temperatures using dynamic mechanical analysis (DMA) (Fig. 4a; Supplementary Section 4.13). The stress-time relationship was well-described by an exponential equation based on rheological theory. The applied stress was released rapidly (relaxation time τ-1 min) at room temperature (25 °C). The frequency sweep of the Ph polymer showed that the storage modulus and loss modulus had a crossover point at 50 rad s^{-1}, indicating that the bond exchange rate was fast at 25 °C[34] (Supplementary Fig. 14a), which aligned well with the fast relaxation behavior observed by DMA. Meanwhile, the modulus versus temperature curves of the Ph polymer showed a rapid decrease in storage modulus as the temperature increased (Supplementary Fig. 14b), suggesting a decreased crosslinking density. These experimental results and theoretical simulation (Fig. 2d) indicate that the relaxation behavior of the crosslinked polymer is based on the fast bond exchange via a dissociative stepwise mechanism[35] (Supplementary Fig. 15).

We then examined the relaxation times at different temperatures using an Arrhenius plot (R^2 > 0.99) and estimated the activation energy of stress relaxation (E_a(sr)) as 36.2 ± 1.5 kJ mol^{-1} (Fig. 4b; Supplementary Section 4.13), which is close to the lowest reported value[19] (31 ± 10 kJ mol^{-1}) for dynamic polymer networks[8–10,13–15,17,19,20,22,23,25,36–46] (Fig. 4c). E_a(sr) was lower than the activation energy of the exchange reaction in solution (E_a(sol) = 80.3 ± 8.3 kJ mol^{-1}; Supplementary Section 4.4), which could be explained by the inherently different mechanism of relaxation in solution and in bulk[35]. The rapid bond exchange rate, low E_a, and relatively low T_g (12.5 °C) of the polymer mean that this material could have excellent dynamic properties at room temperature (~25 °C) or human body temperature (~37 °C).

To test this hypothesis, we cut a sample and gently put two sections together (Fig. 4d, left), and we then traced the self-healing process (25 °C) using a microscope (Fig. 4d and Supplementary Fig. 16a) and mechanical characterization (Fig. 4e) (Supplementary Section 4.14). Without external assistance, the initial crack width (54 μm, Fig. 4d) gradually narrowed to less than 5 μm (Fig. 4d, top right) after only 10 min, achieving more than 90% recovery of the crack (Supplementary Fig. 16b). With added external pressure (~0.1 MPa) at the beginning, the crack was nearly unobservable after 10 min (Fig. 4d, bottom right). The mechanical stiffness of the self-repaired sample gradually increased over a span of less than 10 min until it was almost the same as that of the original sample (Fig. 4e). The breaking stress of the self-healed sample was restored to 90% within 10 min, and a longer self-healing time (e.g., 20 min) affected the repair rate only a little (90 to 93%) (Fig. 4e, inset; Supplementary Fig. 16). The visual and mechanical results demonstrate that this DHPMT-acrylate crosslinked polymer is a dynamic material that self-heals at room temperature, which is rare.

In addition to the dynamic properties, we also explored other functions of the crosslinked polymer derived from the DHPMT heterocycle. We molded the Ph polymer ($M(A_3)$ = 692 g mol^{-1}) into a visually transparent light-yellow film (Ph film, inset photo on the left of Fig. 5a) and evaluated its UV-blocking ability using UV-vis transmittance spectra (Fig. 5a). This Ph film exhibited remarkable blocking ability against UV light (250–400 nm) (blocking rate: >99%), while having good transparency (87%) to visible light (400–760 nm). We also molded the recycled Ph polymer into a film that was darker than the original Ph film (Supplementary Fig. 13d, inset). This recycled film retained excellent UV-blocking ability; however, due to the presence of

https://doi.org/10.1038/s41467-025-59027-3

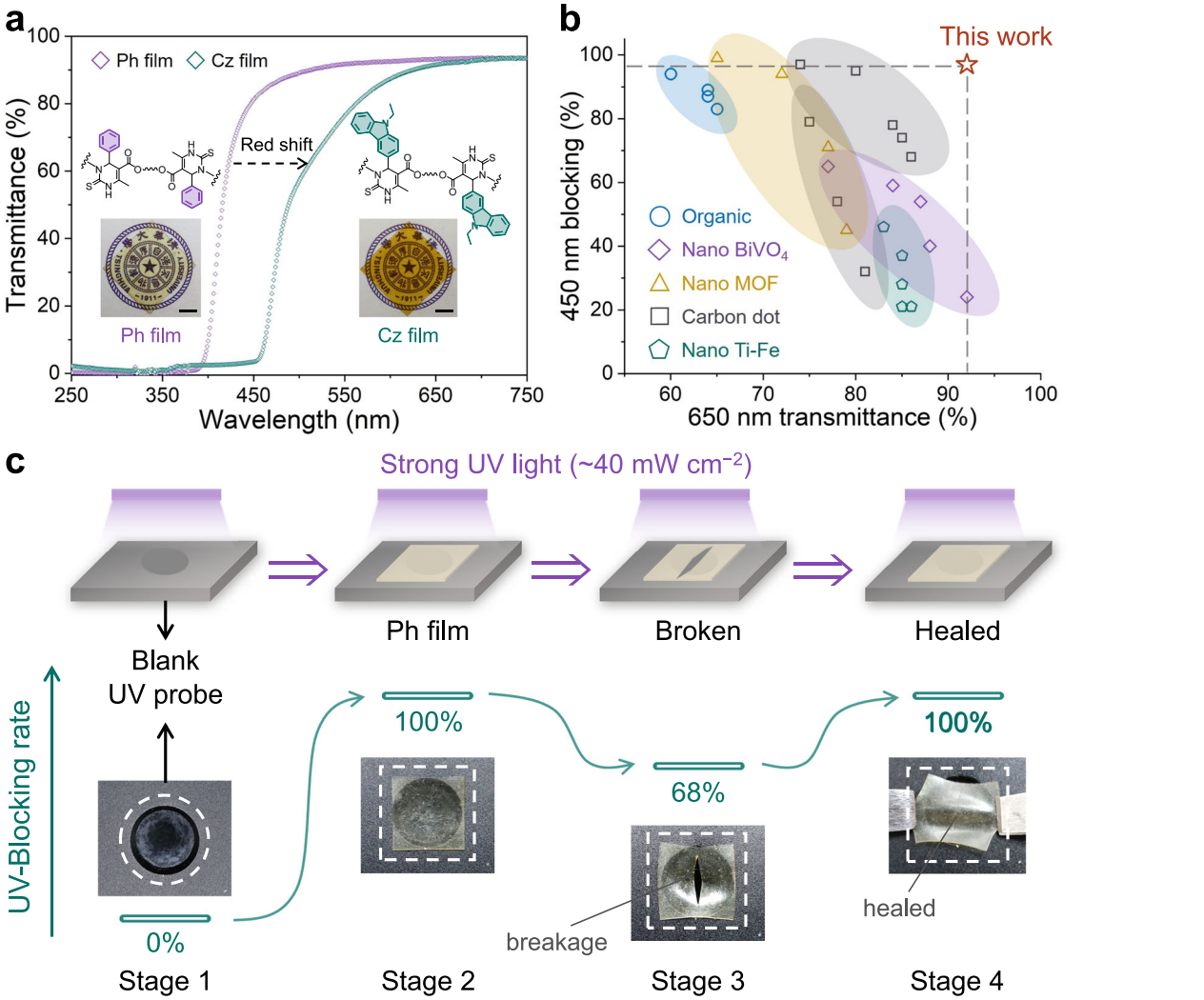

Fig. 5 | Ultraviolet (UV)- and high-energy blue light (HEBL)-shielding properties of the bulk materials. a UV-vis transmittance spectra and photos (inset) of polymer films with a phenyl substituent (Ph film, left) and an *N*-ethyl carbazolyl substituent (Cz film, right), respectively; thickness of the films: 0.20 mm; scale bar = 2.5 mm. **b** Schematic illustration of the process of the wear resistance test (UV light: wavelength = 365 ± 3 nm, power density = 40–42 mW cm^{-2}) of the Ph film (top) with corresponding photos and UV-blocking rates of each stage (bottom). **c** Comparison of the Cz film with recently reported HEBL-shielding films in terms of the HEBL-blocking ability (blocking rate at 450 nm) and visible light transparency (transmittance at 650 nm). Different shadings represent that the data come from different references.

side products, it was less transparent to visible light compared with the original film (Supplementary Fig. 13d).

We evaluated the blocking ability of the Ph film against strong UV light (365 ± 3 nm; 40–42 mW cm^{-2}) (Supplementary Fig. 17; Supplementary Section 4.15). After exposure for 100 h, this Ph film still maintained almost 100% of the UV-blocking rate (Supplementary Fig. 17, stage 3) of the original sample (Supplementary Fig. 17, stage 2), which indicates that the Ph film has excellent blocking ability against strong UV exposure.

We further investigated the wear resistance of the Ph film (Fig. 5b and Supplementary Fig. 18; Supplementary Section 4.15). The Ph film was placed on a blank UV probe under strong UV exposure (365 ± 3 nm; 40–42 mW cm^{-2}) (Fig. 5b, stages 1 to 2), and the real-time power (P_{RT}) immediately dropped to 0 mW cm^{-2} (Supplementary Fig. 18, stages 1 to 2), which indicated that the blocking rate was almost 100%. Then, we cut the Ph film to simulate wear during practical use, and the blocking rate decreased remarkably to 68% (Fig. 5b, stages 2 to 3). After a 10-minute self-healing process at room temperature (25 °C), the film recovered 100% of its UV-shielding ability (Fig. 5b, stages 3 to 4). These results demonstrate that this Ph film has excellent UV-blocking function, and its self-healing property makes it superior to traditional UV-blocking materials in terms of durability. Developing effective UV-shielding films with high transparency and self-healing ability remains a challenge. The current research provides a pathway for fabricating transparent and self-healable UV-resistant polymer films through simple molecular design and synthesis.

Subsequently, we used the crosslinked polymer to develop HEBL-blocking materials by facilely altering the components of the Biginelli reaction. We synthesized a di-DHPMT monomer with an *N*-ethyl carbazolyl substituent (Cz-B_2 monomer) and prepared the corresponding crosslinked polymer (Cz polymer). The CP/MAS ^{13}C NMR and low-field NMR analyses indicated that this polymer had a high crosslinking density through a nearly complete crosslinking reaction (Supplementary Fig. 19; Supplementary Section 4.9). We then hot-pressed the Cz polymer to prepare an orange polymer film (Cz film, inset photo on the right of Fig. 5a). This Cz film is also self-healable (Supplementary Fig. 20), which indicates that changing the structure of DHPMT does not ruin its dynamic properties; this observation is consistent with our previous conclusion. Meanwhile, the UV-vis transmittance curve of this Cz film showed a significant

https://doi.org/10.1038/s41467-025-59027-3

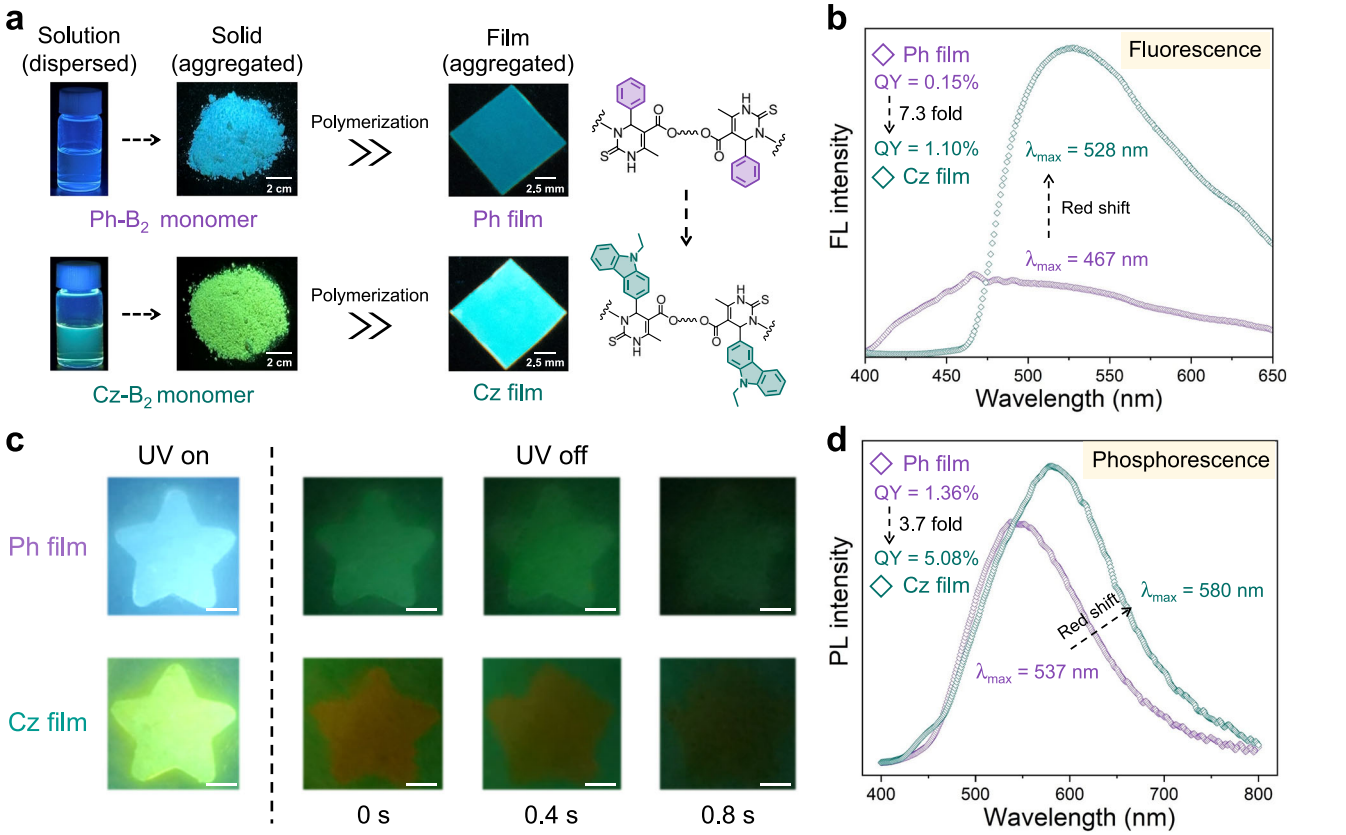

Fig. 6 | Fluorescence and phosphorescence properties of the crosslinked polymers. a Photographs of the monomers (top left: the Ph-B_2 monomer; bottom left: the Cz-B_2 monomer; scale bar = 2 cm) in solution (1 mg mL^{-1} in DMF) and in solid state, and the polymer films (top right: the Ph film; bottom right: the Cz film; thickness: 0.20 mm; scale bar = 2.5 mm) under UV light (365 nm). **b** Fluorescence spectra and quantum yields (QYs) of the Ph film and the Cz film. Excitation wavelength: 365 nm. **c** Photographs of luminescence of the Ph film (top) and the Cz film (bottom) with UV light (365 nm) on (left) and off (right) at 77 K. Scale bar = 0.5 cm. **d** Phosphorescence spectra and QYs of the Ph film and the Cz film at 77 K. Excitation wavelength: 365 nm; delayed time: 30 μs.

red-shift relative to that of the Ph film (Fig. 5a); thus, this Cz film effectively shields HEBL (400–460 nm) (blocking rate: ~97%) in addition to blocking UV light (blocking rate: ~99%). We compared the Cz film with the recently reported HEBL-blocking materials (organic film[47], metal nanoparticles[48,49], metal-organic frameworks[50], and carbon quantum dots[51,52]) in terms of HEBL-blocking ability (blocking rate at 450 nm) and visible light transmittance (transmittance at 650 nm) (Fig. 5c). The Cz film exhibited the highest transparency (92% at 650 nm) among all the comparison materials and a similar high HEBL-blocking rate (97% at 450 nm) to some reported films that have relatively poor transparency (<80% at 650 nm)[47,50,51]. Given the widespread use of electronic devices, prolonged exposure to HEBL is common and is hazardous to eye and skin health[53–55]; thus, the development of HEBL-protection material has been widely sought. The current study introduces a self-healable HEBL-protective material and demonstrates the value of heterocycle-based dynamic functional materials.

Polymers that contain heterocycles, even without conventional luminophores, may also possess unique photophysical properties due to the cluster luminescence mechanism[56–58] (e.g., cellulose). Therefore, we investigated the fluorescence properties of the di-DHPMT monomers and polymers. Under a UV light (365 nm), the solution with Ph-B_2 monomer (1 mg mL^{-1} in DMF) showed negligible fluorescence, whereas the solid Ph-B_2 and the Ph film prepared from the Ph-B_2 were fluorescent (Fig. 6a, top).

Similarly, the fluorescence of the Cz-B_2 monomer in aggregation states (the solid and the Cz film) was much stronger than it was in the solution state (Fig. 6a, bottom). These phenomena agree well with the mechanism of cluster luminescence, i.e., the aggregation state is more favorable toward the intermolecular interactions and molecular cluster formation than the dispersion state.

In the fluorescence spectra (Fig. 6b), the Cz film (λ_{max} = 528 nm) had an apparently red-shifted emission band relative to the Ph film (λ_{max} = 467 nm); the quantum yields (QY) of the Cz film (QY = 1.10%) was 7.3 times that of the Ph film (QY = 0.15%). This may be attributable to the stronger π-π interactions in the Cz film than in the Ph film, which would have produced more rigid molecular clusters in the Cz film and reduced the ratio of non-radiative transitions between the S_1 and S_0 levels[59,60].

We also investigated the phosphorescence properties of the polymer films. Under a 365 nm UV light at 77 K, the Ph film (Fig. 6c, top) and the Cz film (Fig. 6c, bottom) showed blue and yellow-green fluorescence, respectively. After the UV light was turned off, the Ph film emitted a yellow-green afterglow, whereas the Cz film was accompanied by an orange-yellow phosphorescence. Both films exhibited relatively long lifetimes of luminescence according to the photos (Fig. 6c) and the time-resolved phosphorescence decay test (Ph film: τ = 2.50 ms; Cz film: τ = 5.19 ms) (Supplementary Fig. 21), which indicates that these DHPMT-acrylate crosslinked polymers are potential long-afterglow organic materials. The emission band of the Cz film (λ_{max} = 580 nm) was notably red-shifted relative to that of the Ph film (λ_{max} = 537 nm) (Fig. 6d), which is consistent with the results of the phosphorescence experiment. The QY of the Cz film (5.08%) was 3.7 times that of the Ph film (1.36%), which could also be attributed to stronger intermolecular interactions in the Cz film. These results demonstrate that the materials developed via DHPMT-based dynamic reaction have diverse and tunable properties/functions, which are difficult to achieve through traditional DCC.

Discussion

For basic reactions, this study offers insights into the development of dynamic chemistry based on heterocycles. In future research, other heterocycles, especially readily chemically accessible heterocycles such as pyrimidine, purine, imidazole, and indole, could be exploited for different H-DCC. However, a tremendous amount of work is required to carefully screen reactions and substrates to obtain the desired results. For example, we initially preferred dihydropyrimidin-2(1*H*)-one (DHPM) over DHPMT as the substrate; however, the addition reaction between the DHPM model compound (M0′) and methyl acrylate (**a**) produced no target product under the established conditions (Supplementary Fig. 22). Meanwhile, in the present study, we proposed a possible mechanism based only on our experimental results (including some unpresented data) and DFT simulations. In future research, we intend to again use advanced characterizations, such as real-time mass spectrometry, high-resolution mass spectrometry, in-situ infrared spectroscopy, and in-situ NMR spectroscopy, to capture the intermediates and further verify the rationality and universality of the mechanism.

In terms of materials, the current study validates only the use of H-DCC to facilely develop dynamic functional materials that are difficult to develop through traditional DCC. In the future, we may optimize the properties and extend the scale of application of DHPMT-acrylate dynamic materials according to application requirements. We have successfully prepared crosslinked polymers using different monomers. These polymers have excellent thermal stability (Supplementary Fig. 23) and a wide range of T_gs (Supplementary Fig. 24), as well as diverse mechanical properties (Supplementary Figs. 25, 26 and Supplementary Table 9). Besides, we have demonstrated that the polymer network is recyclable; however, the depolymerization of the polymer network cannot proceed completely and is accompanied by inevitable side reactions under current conditions. In future research, we may explore other pathways for the degradation of the polymer networks to eliminate side products and realize thorough depolymerization, thus achieving closed-loop recycling or upcycling of the polymer networks.

It is also possible to endow the DHPMT-acrylate polymers with other appealing functions, such as super-wettability, stimuli-response ability, and metal-chelating ability, by altering the moiety of the Biginelli reaction or changing the chain structures and improve the QYs of the fluorescence/phosphorescence of the polymers by carefully designing the functional groups and molecular rigidness of the polymers. Moreover, other functions of the DHPMT heterocycle, such as anti-bacterial and anti-viral functions, as well as anti-oxidation, may also be combined with its dynamic properties to develop multifunctional and dynamic materials.

In summary, we studied H-DCC and developed a strategy to facilely explore dynamic functional materials. We uncovered the reversibility of the aza-Michael addition reaction between DHPMT and acrylate through model experiments and theoretical calculations. Based on this dynamic aza-Michael addition reaction, the linear polymer prepared using DHPMT-acrylate chemistry was almost completely degraded into monomers, which demonstrates its potential as a degradable polymer. The crosslinked polymer demonstrated recyclability and dynamic properties (degradability, and suitability for repeated reprocessing and reshaping) similar to those of traditional DCC-based materials. It also exhibited a fast relaxation rate (τ ~ 1 min) and low activation energy ($E_a = 36.2 \pm 1.5$ kJ mol^{-1}), which gave it a good self-healing ability (recovery rate: ~90% in 10 min) at room temperature (~25 °C).

We then combined the dynamic properties of DHPMT-acrylate and the intrinsic functions of DHPMT to fabricate dynamic functional materials. We used the crosslinked polymer to prepare a self-healable Ph film with excellent UV-shielding capacity (blocking rate: >99% for UV light) and high transparency (87% for visible light). By simply altering the components of the Biginelli reaction, we obtained a Cz film that was also self-healable and superior in HEBL-blocking ability (97% at 450 nm) and transparency (92% at 650 nm) to recently reported HEBL-blocking materials. The Ph film and Cz film were fluorescent under UV light due to the cluster luminescence mechanism; they also emitted phosphorescence when the UV light was turned off.

This proof-of-concept research verifies the feasibility of H-DCC and successfully develops dynamic optical materials that cannot be easily prepared directly by conventional DCC, thereby demonstrating the advantages of H-DCC in exploring dynamic functional materials. These advantages may prompt an in-depth study of reversible heterocycle-based reactions, as well as a systematic theory of H-DCC and dynamic functional polymer materials using different heterocycles.

Methods

Materials

All chemicals, reagents, and solvents were purchased from commercial sources. Ethyl acetoacetate (General Reagent, 98%), *tert*-butyl acetoacetate (Bidepharm, 99%), thiourea (Meryer, 99%), benzaldehyde (Energy, 99%), benzyl acrylate (Bidepharm, ≥99%), benzyl methacrylate (Heowns, 98%), *N*-benzylacrylamide (Bidepharm, 97%), phenyl vinyl sulfone (Bidepharm, ≥99%), acrylonitrile (Macklin, 99%), *N*-methylthiourea (Aladdin, 98%), benzyl acetoacetate (Bidepharm, 98%), *p*-anisaldehyde (Bidepharm, 99%), 1,8-octanediol (J&K Scientific, 98%), *N*-ethyl-3-carbazolecarboxaldehyde (Aladdin, 98%), chlorotrimethylsilane (J&K Scientific, 98%), ethoxylated trimethylolpropane tri-acrylate (A_3 monomer, molecular weight: 428, 692, or 912 g mol^{-1}, Aladdin), 1,6-dibromohexane (Aladdin, 97%), 4-hydroxybenzaldehyde (Bidepharm, 98%), 1,8-diazabicyclo[5.4.0]undec-7-ene (Bidepharm, ≥99%), *N*,*N*-dimethylformamide (Tongguang, ≥99.5%), dimethyl sulfoxide (Tongguang, ≥99.5%), tetrahydrofuran (Tongguang, ≥99.5%), and dichloromethane (General Reagent, ≥99%) were used as received. Hexane-1,6-diyl diacrylate (Bidepharm, 90%) was purified by silica gel chromatography (petroleum ether) prior to use.

Instrumental analysis

Gel permeation chromatography (GPC) analyses of polymers were performed using *N*,*N*-dimethylformamide (DMF) with 50 mM LiBr as the eluent. The GPC system employed a Shimadzu LC-20AD pump with an auto-injector, a PLgel 5 μm guard column (50 × 7.5 mm), followed by three PLgel 5 μm MIXED-D columns (300 × 7.5 mm). Detection was achieved using a Shimadzu RID-20A refractive index detector and a Shimadzu SPD-20A UV detector. The GPC system was calibrated with polystyrene standards of narrow molecular weight distribution (M_n: 1300 to 2630,000 g mol^{-1}). All GPC samples were prepared with a concentration of 5 mg mL^{-1} unless otherwise specified. Liquid-state ^{1}H and ^{13}C nuclear magnetic resonance (NMR) spectra were acquired using a JEOL JNM-ECA400 (400 MHz) spectrometer for all samples. Solid-state cross-polarization magic-angle spinning (CP/MAS) ^{13}C NMR spectra were acquired using a JEOL JNM-ECA600 (600 MHz) spectrometer. Low-field NMR relaxation decay curves were acquired on a Niumag VTMR20-010V-I (21 MHz) spectrometer. Fourier transform infrared (FT-IR) spectra were collected in attenuated total reflection (ATR) mode on a PerkinElmer Spectrum 100 FT-IR spectrometer. Temperature variable FT-IR spectra were obtained in transmittance mode on a Thermo Fisher Nicolet iS50 FT-IR spectrometer. UV-visible (UV-vis) transmittance spectra were acquired with a PerkinElmer Lambda 750 spectrometer. Fluorescence spectra were obtained using a Shimadzu RF-6000 Spectro fluorophotometer equipped with quartz cuvettes. Phosphorescence spectra and time-resolved phosphorescence decay measurements were conducted using an Edinburgh FLS1000 photoluminescence spectrometer. Electron spray ionization ion trap/time-of-flight mass spectra (ESI-IT/TOF MS) were performed on a Shimadzu LCMS-IT-

TOF system. Differential scanning calorimetry (DSC) was performed using TA Instruments Q2000 at a scanning rate of 10 °C min^{-1}. Dynamic mechanical analysis (DMA) results were acquired on a TA Instruments Q800 machine. Rheological analyses were performed on a TA AR2000ex rheometer. Thermogravimetric analyses (TGA) were conducted using a BeiguangHongyuan WRT-121 thermogravimetric analyzer with a heating rate of 10 °C min^{-1}. Mechanical stiffness and pull-off tests were performed on an INSTRON R3178 universal testing system. The UV-blocking ability was tested by a SCOUT UVLED (NX3035-15K, Yancheng Nuoxi Electronic Equipment Co. Ltd.) UV light (365 ± 3 nm) and a UV radiometer (WKM-UV1, detecting wavelength: 340–410 nm). The microscopic images were collected with a Nikon Eclipse LV100POL polarizing optical microscope.

Preparation of DHPMT model compounds (M0, M1, M2, and M3)

As a typical example, benzaldehyde (0.531 g, 5.0 mmol), ethyl acetoacetate (0.651 g, 5.0 mmol), and thiourea (0.571 g, 7.5 mmol) were dissolved in *N*,*N*-dimethylformamide (DMF, 2.5 mL) in a round-bottom flask. Chlorotrimethylsilane (TMSCl, 1.09 g, 10 mmol) was then added dropwise at room temperature (~25 °C). The mixture was heated to 80 °C and stirred for 2 h, then precipitated into cold water under stirring. The resulting precipitate was collected by suction filtration and washed three times with water to yield M0 as a white solid (2.02 g, 92% yield).

M1 (yellow solid, 90% yield), M2 (orange solid, 90% yield), and M3 (white solid, 85% yield) were similarly prepared.

Density functional theory (DFT) simulation

All calculations were performed using the Gaussian 16 software package[61]. Geometry optimizations were conducted at the B3LYP[62]-D3(BJ)[63]/def2-SVP[64] level of theory. Frequency calculations were carried out at the same level of theory to obtain Gibbs free energy corrections and to identify all the stationary points as either minima (no imaginary frequency) or transition states (one imaginary frequency). Higher-level single-point energies were calculated using M06-2X[65]-D3[63]/def2-TZVP[64]. Solvation effects in DMSO were taken into consideration using the SMD[66] implicit solvation model in all calculations. A concentration correction of 1.9 kcal mol^{-1} at room temperature (derived from the free energy change when transitioning from 1 mol of an ideal gas at 1 atm to 1 mol L^{-1} in DMSO) was applied to all species.

Degradation of the linear polymer P1

P1 (0.009 g, *n*(DHPMT) = 0.02 mmol) was dissolved in 10 mL of solvent (DMSO-d_6 or DMF). The solution was heated to 120 °C, and then sodium *tert*-butoxide (^{t}BuONa, 0.002 g, 0.02 mmol) was added as the base. Samples were taken at different time intervals for ^{1}H NMR (using DMSO-d_6 as solvent) or GPC (using DMF as solvent) analyses to monitor the degradation process.

Preparation of the Ph-B_2 monomer and the Cz-B_2 monomer

1,8-Octanediol (16.1 g, 110 mmol) and tert-butyl acetoacetate (31.6 g, 200 mmol) were dissolved in toluene (100 mL). The mixture was refluxed at 110 °C for 16 h followed by removing toluene using rotary evaporation. The residue was purified via a quick silica chromatography (ethyl acetate/petroleum ether = 1/20 to 1/10) to produce octane-1,8-diyl bis(3-oxobutanoate) (di-keto) as a colorless oil (29.6 g, 94% yield).

The obtained di-keto (3.14 g, 10 mmol), thiourea (2.28 g, 30 mmol), and benzaldehyde (2.12 g, 20 mmol) were dissolved in DMF (10 mL), then TMSCl (4.35 g, 40 mmol) was added dropwise to the mixture at room temperature (~25 °C). The mixture was stirred at 80 °C for 2 h, then precipitated into cold water. The sediment was recrystallized in isopropyl alcohol to obtain the Ph-B_2 monomer as a white solid (5.22 g, 86% yield). The Cz-B_2 monomer was similarly prepared as a bright yellow solid (7.41 g, 88% yield) using *N*-ethyl-3-carbazolecarboxaldehyde instead of benzaldehyde.

Preparation of the bulk materials and polymer films

Bulk materials. Tri-acrylate monomer (A_3 monomer, 1.0 mmol) and di-DHPMT monomer (Ph-B_2 monomer: 0.91 g, 1.5 mmol or Cz-B_2 monomer: 1.51 g, 1.8 mmol) were mixed in a silicon rubber mold (5 cm × 5 cm) and stirred on a thermal plate (set at 160 °C) until homogenous. The mold was removed from the thermal plate, and DBU (0.034 g, 0.225 mmol, i.e., 0.075 eq relative to the DHPMT groups) was added dropwise into the mixture under vigorous stirring. The mixture became highly viscous or solid within 0.5–1 min, then the rubber mold was put back on the thermal plate and heated for additional 10 min for complete polymerization. The crosslinked polymer was obtained as a light-yellow (the Ph polymer) or orange (the Cz polymer) bulk material. The molecular weight of A_3 monomer as well as the feed ratio of A_3 monomer and B_2 monomer can be adjusted to obtain polymers with different properties.

Polymer films. The as-prepared bulk materials were hot-pressed at 160 °C under 2 MPa for 10 min to obtain a transparent light-yellow film (the Ph film) or orange film (the Cz film).

Chemical resistance and gel content test

Small rectangular samples (15 mm (*L*) × 3.0 mm (*W*) × 0.2 mm (*T*)) of the Ph polymer ($M(A_3)$ = 692 g mol^{-1}) were immersed in 0.1 M HCl (aq), 0.1 M NaOH (aq), 3 wt% NaCl (aq), tetrahydrofuran (THF), dichloromethane (DCM), ethanol (EtOH), and DMF, respectively. The samples were kept in these solvents at 25 °C for 24 h, then the solvents were drained, and the remaining residues were dried in an oven (100 °C) for 24 h. The weights of the samples were measured before and after the test to determine the gel content in each solvent following the method in Supplementary Section 4.10.

Reprocessing and reshaping experiments of the bulk material

Reprocessing. A Ph film ($M(A_3)$ = 428 g mol^{-1}) was fragmented into small pieces. These polymer fragments were then reprocessed by hot pressing (160 °C, 2 MPa) to form a uniform polymer film. This fragmentation-reprocessing cycle could be conducted repeatedly.

Reshaping. A Ph film ($M(A_3)$ = 692 g mol^{-1}) was cut into a strip (35 mm (*L*) × 3.0 mm (*W*) × 0.2 mm (*T*)). This strip was spirally wound around a metal bar with both ends held by tapes. The metal bar along with the sample was heated in an electric heating jacket (100 °C) for 5 min, then cooled to room temperature (~25 °C). The sample was removed from the metal bar, and the permanent shape of the sample was turned to helix.

Self-healing test

A rectangular Ph film ($M(A_3)$ = 692 g mol^{-1}) sample (20 mm (*L*) × 3.0 mm (*W*) × 0.2 mm (*T*)) was cut into two equal pieces along its length. These two sections were placed on a flat surface and gently touched at room temperature (~25 °C). For the pressure-assisted healing test, a vertical pressure (~0.1 MPa) was applied to the two pieces of sample during the healing process. Multiple sets of self-healing tests were parallelly performed. After different healing times (0, 2, 5, 10, and 20 min), the microscopic images and the mechanical data of the samples were collected to monitor the healing process. The recovery rate at a certain time was calculated following the method in Supplementary Section 4.14.

Data availability

Data supporting the findings of this study are included in the Article and its Supplementary Information. All data are available upon request.

References

1. Scheutz, G. M., Lessard, J. J., Sims, M. B. & Sumerlin, B. S. Adaptable crosslinks in polymeric materials: resolving the intersection of thermoplastics and thermosets. *J. Am. Chem. Soc.* **141**, 16181–16196 (2019).
2. Korley, L. T. J., Epps, T. H., Helms, B. A. & Ryan, A. J. Toward polymer upcycling—adding value and tackling circularity. *Science* **373**, 66–69 (2021).
3. Zheng, N., Xu, Y., Zhao, Q. & Xie, T. Dynamic covalent polymer networks: a molecular platform for designing functions beyond chemical recycling and self-healing. *Chem. Rev.* **121**, 1716–1745 (2021).
4. Lei, Z. et al. New advances in covalent network polymers via dynamic covalent chemistry. *Chem. Rev.* **124**, 7829–7906 (2024).
5. Nicholson, S. R., Rorrer, N. A., Carpenter, A. C. & Beckham, G. T. Manufacturing energy and greenhouse gas emissions associated with plastics consumption. *Joule* **5**, 673–686 (2021).
6. Chen, E. Y. X. Factoring timescale in for sustainable polymer design. *Nat. Sustain.* **6**, 1140–1141 (2023).
7. Borrelle, S. B. et al. Predicted growth in plastic waste exceeds efforts to mitigate plastic pollution. *Science* **369**, 1515–1518 (2020).
8. Montarnal, D., Capelot, M., Tournilhac, F. & Leibler, L. Silica-like malleable materials from permanent organic networks. *Science* **334**, 965–968 (2011).
9. Cromwell, O. R., Chung, J. & Guan, Z. Malleable and self-healing covalent polymer networks through tunable dynamic boronic ester bonds. *J. Am. Chem. Soc.* **137**, 6492–6495 (2015).
10. Röttger, M. et al. High-performance vitrimers from commodity thermoplastics through dioxaborolane metathesis. *Science* **356**, 62–65 (2017).
11. He, C., Shi, S., Wang, D., Helms, B. A. & Russell, T. P. Poly(oxime–ester) vitrimers with catalyst-free bond exchange. *J. Am. Chem. Soc.* **141**, 13753–13757 (2019).
12. Clarke, R. W. et al. Dynamic crosslinking compatibilizes immiscible mixed plastics. *Nature* **616**, 731–739 (2023).
13. Obadia, M. M., Mudraboyina, B. P., Serghei, A., Montarnal, D. & Drockenmuller, E. Reprocessing and recycling of highly cross-linked ion-conducting networks through transalkylation exchanges of C–N bonds. *J. Am. Chem. Soc.* **137**, 6078–6083 (2015).
14. Hendriks, B., Waelkens, J., Winne, J. M. & Du Prez, F. E. Poly(-thioether) vitrimers via transalkylation of trialkylsulfonium salts. *ACS Macro Lett.* **6**, 930–934 (2017).
15. Obadia, M. M., Jourdain, A., Cassagnau, P., Montarnal, D. & Drockenmuller, E. Tuning the viscosity profile of ionic vitrimers incorporating 1,2,3-triazolium cross-links. *Adv. Funct. Mater.* **27**, 1703258 (2017).
16. Taynton, P. et al. Heat- or water-driven malleability in a highly recyclable covalent network polymer. *Adv. Mater.* **26**, 3938–3942 (2014).
17. Denissen, W. et al. Vinylogous urethane vitrimers. *Adv. Funct. Mater.* **25**, 2451–2457 (2015).
18. Chao, A., Negulescu, I. & Zhang, D. Dynamic covalent polymer networks based on degenerative imine bond exchange: tuning the malleability and self-healing properties by solvent. *Macromolecules* **49**, 6277–6284 (2016).
19. Denissen, W. et al. Chemical control of the viscoelastic properties of vinylogous urethane vitrimers. *Nat. Commun.* **8**, 14857 (2017).
20. Christensen, P. R., Scheuermann, A. M., Loeffler, K. E. & Helms, B. A. Closed-loop recycling of plastics enabled by dynamic covalent diketoenamine bonds. *Nat. Chem.* **11**, 442–448 (2019).
21. Genest, A., Portinha, D., Fleury, E. & Ganachaud, F. The aza-Michael reaction as an alternative strategy to generate advanced silicon-based (macro)molecules and materials. *Prog. Polym. Sci.* **72**, 61–110 (2017).
22. Van Herck, N. et al. Covalent adaptable networks with tunable exchange rates based on reversible thiol-yne cross-linking. *Angew. Chem. Int. Ed.* **59**, 3609–3617 (2020).
23. Taplan, C., Guerre, M. & Du Prez, F. E. Covalent adaptable networks using β-amino esters as thermally reversible building blocks. *J. Am. Chem. Soc.* **143**, 9140–9150 (2021).
24. Lee, G. et al. Harnessing β-hydroxyl groups in poly(β-amino esters) toward robust and fast reprocessing covalent adaptable networks. *Macromolecules* **55**, 10366–10376 (2022).
25. Crolais, A. E. et al. Enhancing the equilibrium of dynamic thia-michael reactions through heterocyclic design. *J. Am. Chem. Soc.* **145**, 14427–14434 (2023).
26. Li, J. & Pu, K. Development of organic semiconducting materials for deep-tissue optical imaging, phototherapy and photoactivation. *Chem. Soc. Rev.* **48**, 38–71 (2019).
27. Bhutani, P. et al. U.S. FDA aproved drugs from 2015–June 2020: a perspective. *J. Med. Chem.* **64**, 2339–2381 (2021).
28. Kovachka, S. et al. Small molecule approaches to targeting RNA. *Nat. Rev. Chem.* **8**, 120–135 (2024).
29. Boncel, S., Mączka, M. & Walczak, K. Z. Michael versus retro-Michael reaction in the regioselective synthesis of N-1 and N-3 uracil adducts. *Tetrahedron* **66**, 8450–8457 (2010).
30. Ma, Z. et al. Introducing the aza-Michael addition reaction between acrylate and dihydropyrimidin-2(1H)-thione into polymer chemistry. *Polym. Chem.* **13**, 6322–6327 (2022).
31. Wang, X., Quan, Z., Wang, J.-K., Zhang, Z. & Wang, M. A practical and green approach toward synthesis of N3-substituted dihydropyrimidinones: using aza-Michael addition reaction catalyzed by KF/Al2O3. *Bioorg. Med. Chem. Lett.* **16**, 4592–4595 (2006).
32. Nagarajaiah, H., Mukhopadhyay, A. & Moorthy, J. N. Biginelli reaction: an overview. *Tetrahedron Lett.* **57**, 5135–5149 (2016).
33. Matos, L. H. S., Masson, F. T., Simeoni, L. A. & Homem-de-Mello, M. Biological activity of dihydropyrimidinone (DHPM) derivatives: a systematic review. *Eur. J. Med. Chem.* **143**, 1779–1789 (2018).
34. Podgórski, M. et al. Toward stimuli-responsive dynamic thermosets through continuous development and improvements in covalent adaptable networks (CANs). *Adv. Mater.* **32**, 1906876 (2020).
35. Winne, J. M., Leibler, L. & Du Prez, F. E. Dynamic covalent chemistry in polymer networks: a mechanistic perspective. *Polym. Chem.* **10**, 6091–6108 (2019).
36. Brutman, J. P., Delgado, P. A. & Hillmyer, M. A. Polylactide vitrimers. *ACS Macro Lett.* **3**, 607–610 (2014).
37. Fortman, D. J., Brutman, J. P., Cramer, C. J., Hillmyer, M. A. & Dichtel, W. R. Mechanically activated, catalyst-free polyhydroxyurethane vitrimers. *J. Am. Chem. Soc.* **137**, 14019–14022 (2015).
38. Ruiz de Luzuriaga, A. et al. Epoxy resin with exchangeable disulfide crosslinks to obtain reprocessable, repairable and recyclable fiber-reinforced thermoset composites. *Mater. Horiz.* **3**, 241–247 (2016).
39. Zheng, N., Fang, Z., Zou, W., Zhao, Q. & Xie, T. Thermoset shape-memory polyurethane with intrinsic plasticity enabled by transcarbamoylation. *Angew. Chem. Int. Ed.* **55**, 11421–11425 (2016).
40. Nishimura, Y., Chung, J., Muradyan, H. & Guan, Z. Silyl ether as a robust and thermally stable dynamic covalent motif for malleable polymer design. *J. Am. Chem. Soc.* **139**, 14881–14884 (2017).
41. Ishibashi, J. S. A. & Kalow, J. A. Vitrimeric silicone elastomers enabled by dynamic Meldrum's acid-derived cross-links. *ACS Macro Lett.* **7**, 482–486 (2018).
42. Snyder, R. L., Fortman, D. J., De Hoe, G. X., Hillmyer, M. A. & Dichtel, W. R. Reprocessable acid-degradable polycarbonate vitrimers. *Macromolecules* **51**, 389–397 (2018).
43. Yang, Y. et al. Reprocessable thermoset soft actuators. *Angew. Chem. Int. Ed.* **58**, 17474–17479 (2019).
44. Qin, B. et al. Closed-loop chemical recycling of cross-linked polymeric materials based on reversible amidation chemistry. *Nat. Commun.* **13**, 7595 (2022).
45. Fenimore, L. M., Chen, B. & Torkelson, J. M. Simple upcycling of virgin and waste polyethylene into covalent adaptable networks:

catalyst-free, radical-based reactive processing with dialkylamino disulfide bonds. *J. Mater. Chem. A* **10**, 24726–24745 (2022).
46. Lei, Z. et al. Recyclable and malleable thermosets enabled by activating dormant dynamic linkages. *Nat. Chem.* **14**, 1399–1404 (2022).
47. Li, S. et al. A cellulose-based light-management film incorporated with benzoxazine resin/tannic acid exhibiting UV/blue light double blocking and enhanced mechanical property. *Int. J. Biol. Macromol.* **278**, 134461 (2024).
48. Yang, Y. et al. Transparent nanostructured BiVO4 double films with blue light shielding capabilities to prevent damage to ARPE-19 cells. *ACS Appl. Mater. Interfaces* **12**, 20797–20805 (2020).
49. Baimanova, R., Luo, F. & Yang, M. Preparation of iron-doped titania nanoparticles and their UV-blue light-shielding capabilities in polyurethane. *Materials* **15**, 7370 (2022).
50. Sun, L., Li, L., An, X. & Qian, X. Nano-metal organic framework for enhanced mechanical, flame retardant and ultraviolet-blue light shielding properties of transparent cellulose-based bioplastics. *Polymers* **13**, 2433 (2021).
51. Han, Y. et al. Seeking eye protection from biomass: carbon dot-based optical blocking films with adjustable levels of blue light blocking. *J. Colloid Interface Sci.* **617**, 44–52 (2022).
52. Park, S. W., Im, S. H., Hong, W. T., Yang, H. K. & Jung, Y. K. Lignin-derived carbon quantum dot/PVA films for totally blocking UV and high-energy blue light. *Int. J. Biol. Macromol.* **268**, 131919 (2024).
53. Ham, W. T. Jr, Mueller, H. A. & Sliney, D. H. Retinal sensitivity to damage from short wavelength light. *Nature* **260**, 153–155 (1976).
54. Setlow, R. B., Grist, E., Thompson, K. & Woodhead, A. D. Wavelengths effective in induction of malignant melanoma. *Proc. Natl. Acad. Sci. USA* **90**, 6666–6670 (1993).
55. Ouyang, X. et al. Mechanisms of blue light-induced eye hazard and protective measures: a review. *Biomed. Pharmacother.* **130**, 110577 (2020).
56. Tomalia, D. A. et al. Non-traditional intrinsic luminescence: inexplicable blue fluorescence observed for dendrimers, macromolecules and small molecular structures lacking traditional/conventional luminophores. *Prog. Polym. Sci.* **90**, 35–117 (2019).
57. Zhao, W., He, Z. & Tang, B. Z. Room-temperature phosphorescence from organic aggregates. *Nat. Rev. Mater.* **5**, 869–885 (2020).
58. Tang, S. et al. Nonconventional luminophores: characteristics, advancements and perspectives. *Chem. Soc. Rev.* **50**, 12616–12655 (2021).
59. Chu, B. et al. Altering chain flexibility of aliphatic polyesters for yellow-green clusteroluminescence in 38 % quantum yield. *Angew. Chem. Int. Ed.* **61**, e202114117 (2021).
60. Zhu, T., Yang, T., Zhang, Q. & Yuan, W. Z. Clustering and halogen effects enabled red/near-infrared room temperature phosphorescence from aliphatic cyclic imides. *Nat. Commun.* **13**, 2658 (2022).
61. Frisch, M. J. et al. Gaussian 16 Rev. C.01. (2016).
62. Stephens, P. J., Devlin, F. J., Chabalowski, C. F. & Frisch, M. J. Ab initio calculation of vibrational absorption and circular dichroism spectra using density functional force fields. *J. Phys. Chem.* **98**, 11623–11627 (1994).
63. Grimme, S., Ehrlich, S. & Goerigk, L. Effect of the damping function in dispersion corrected density functional theory. *J. Comput. Chem.* **32**, 1456–1465 (2011).
64. Weigend, F. & Ahlrichs, R. Balanced basis sets of split valence, triple zeta valence and quadruple zeta valence quality for H to Rn: design and assessment of accuracy. *Phys. Chem. Chem. Phys.* **7**, 3297–3305 (2005).
65. Zhao, Y. & Truhlar, D. G. The M06 suite of density functionals for main group thermochemistry, thermochemical kinetics, noncovalent interactions, excited states, and transition elements: two new functionals and systematic testing of four M06-class functionals and 12 other functionals. *Theor. Chem. Acc.* **120**, 215–241 (2007).
66. Marenich, A. V., Cramer, C. J. & Truhlar, D. G. Universal solvation model based on solute electron density and on a continuum model of the solvent defined by the bulk dielectric constant and atomic surface tensions. *J. Phys. Chem. B* **113**, 6378–6396 (2009).

Acknowledgements

This research was supported by the National Science Foundation of China (22471140 (L.T.), 22175106 (Y.Y.)), the Key Research and Development Plan (2022YFB3804901 (L.T.)), and the Young Elite Scientists Sponsorship Program by CAST (YESS20230470 (Y.Y.)). The authors thank Mr. Yuhua Guo for the help with theoretical simulation, and Prof. Zhiwu Yu, Prof. Xingwei Guo, Dr. Shiqi Wang, Dr. Chongyu Zhu, Dr. Yahe Wu, Dr. Huan Liang, Mr. Qingyu Meng, Mr. Nankai An, and Mr. Jiantao Zhao for discussion.

Author contributions

L.T. and Z.M. conceived the concept and led the project. Z.M., Y.Z., and B.W. performed the fundamental reaction study. Z.M. performed polymer synthesis, characterization, and demonstration of functions of polymers. Y.Y. performed the dynamic mechanical analysis. S.P. performed the UV-blocking test. L.T. and Z.M. wrote the manuscript. L.T., B.W., and Y.W. provided resources and financial support. All authors discussed and revised the manuscript.

Competing interests

The authors declare no competing interests.

Additional information

Supplementary information The online version contains supplementary material available at https://doi.org/10.1038/s41467-025-59027-3.

Correspondence and requests for materials should be addressed to Bo Wang or Lei Tao.

Peer review information *Nature Communications* thanks the anonymous reviewer(s) for their contribution to the peer review of this work. A peer review file is available.